Journal of Nuclear Materials 385 (2009) 629–632

Contents lists available at ScienceDirect

Journal of Nuclear Materials

journal homepage: www.elsevier.com/locate/jnucmat

Letter to the Editors

Size dependent enhancement of helium ion irradiation tolerance in sputtered Cu/V nanolaminates

E.G. Fu [a], J. Carter [b], G. Swadener [c], A. Misra [c], L. Shao [b], H. Wang [d], X. Zhang [a,*]

[a] Department of Mechanical Engineering, Materials Science and Engineering Program, Texas A&M University, College Station, TX 77843-3123, United States
[b] Department of Nuclear Engineering, Texas A&M University, College Station, TX 77843-3133, United States
[c] Materials Physics and Applications Division, Los Alamos National Laboratory, Los Alamos, NM 87545, United States
[d] Department of Electrical and Computer Engineering, Texas A&M University, College Station, TX 77843-3128, United States

ARTICLE INFO

Article history:
Received 11 November 2008
Accepted 17 December 2008

ABSTRACT

We have investigated the evolution of radiation damage and changes in hardness of sputter-deposited Cu/V nanolaminates upon room temperature helium ion irradiation. As the individual layer thickness decreases from 200 to 5 nm, helium bubble density and radiation hardening both decrease. The magnitude of radiation hardening becomes negligible for individual layer thickness of 2.5 nm or less. These observations indicate that nearly immiscible Cu/V interface can effectively absorb radiation-induced point defects and reduce their concentrations.

1. Introduction

Neutron radiation typically induces significant displacement damage in structural metals, and consequently leads to the formation of point defects (vacancies and interstitials), and their clusters [1–3]. Macroscopically, void swelling frequently occurs in structural steels as a result of the growth of vacancy clusters [4,5]. In parallel, transmutation products such as helium combine with vacancy clusters to form bubbles. Significant void swelling, ~14%, has been observed in neutron irradiated 316 L stainless steels [6]. Degradation of mechanical properties, manifested as radiation-induced embrittlement and loss of ductility, is a serious challenge to the application of structural alloys in nuclear reactors. Early studies on neutron irradiated FCC (such as Cu) and BCC (such as V) metals show that pronounced hardening is due to the presence of radiation-induced point defects, dislocation loops, stacking fault tetrahedra (SFT), and He bubbles [7–9].

In general a scientific approach that reduces the concentration of radiation-induced defects is likely to improve the structural and mechanical integrity, and dimensional stability of reactor alloys. Recently He ion irradiation damage has been studied in Cu/Nb nanolaminates. He bubbles were observed to align along layer interfaces [10,11], and Cu 4 nm/Nb 4 nm nanolaminates were very resistant to blistering (burst of He bubbles) during annealing [10]. Little He bubbles were detected in He ion irradiated Cu 2.5 nm/Nb 2.5 nm specimens [11]. Layer interfaces (phase boundaries) in these nanolaminates may act as sinks for point defects and their clusters [12]. Increasing the volume fraction of atoms at interfaces, by reducing individual layer thickness, thus appears beneficial to alleviating radiation-induced damage. Molecular dynamics (MD) simulation studies suggest that due to their distinctive structure, flat immiscible Cu/Nb interfaces do not support compact, well-localized point defects, which are the primary form of radiation damage in crystals. Instead, these interfaces can accumulate large fluxes of vacancies and interstitials and enhance their recombination, allowing Cu/Nb nanocomposites to persist in a damage-free steady state during intense particle radiation [13]. In spite of these studies, the influence of length scale and the role of different interface types (e.g. Cu/Nb and Cu/V) on void swelling and radiation hardening in irradiated nanolaminates remain unclear. In this study, Cu/V nanolaminates with nearly immiscible interfaces are studied with an attempt to address these questions.

2. Experimental

Cu/V nanolaminates with different individual layer thicknesses were prepared by DC magnetron sputtering technique at room temperature on Si (100) substrates. The total film thickness was approximately 2 μm. Details of synthesis can be found elsewhere [14]. Samples were irradiated with 50 keV He ions to a total fluence of 6×10^{20} ions/m^2 at room temperature for 4 h. The temperature increase of specimens due to beam heating was estimated to be less than 50 °C. The microstructure of Cu/V nanolaminates was characterized by using a JEOL 2010 transmission electron microscope (TEM). The step height between radiated and masked region (to avoid radiation) was measured by a Dektak 3 Stylus profilometer with a resolution of less than 1 nm to detect dimensional change (swelling) of radiated specimens. The hardness and indentation modulus of films were measured (top–down) by using a

* Corresponding author. Tel.: +1 979 845 2143; fax: +1 979 862 2418.
E-mail address: zhangx@tamu.edu (X. Zhang).

0022-3115/$ - see front matter © 2008 Elsevier B.V. All rights reserved.
doi:10.1016/j.jnucmat.2008.12.308

Fischerscope HM2000XYp micro-indenter with a Vicker's indenter. Hardness and elastic modulus were measured at different indentation depths, based on an average of 9–12 indents, and the maximum indentation depth was kept at ~200 nm for all specimens.

3. Results

Cross-sectional TEM (XTEM) images of as-deposited Cu/V 50 nm and Cu/V 2.5 nm nanolaminates in Fig. 1(a) and (b), respectively, show that the interfaces between Cu and V layers are sharp. The inserted selected-area diffraction (SAD) patterns indicate that both layers are polycrystalline with Kurdjumov–Sachs (K–S) orientation relationship, i.e. Cu {1 1 1} // V {1 1 0} and Cu <1 1 0> // V <1 1 1>. The fiber texture, Cu {1 1 1} // V {1 1 0} // interface plane, gets stronger with decreasing layer thickness from 50 to 2.5 nm. Fig. 1(c) and (d) show the under-focus XTEM images of these specimens after He ion irradiation. Superimposed on the images are two depth profiles of He concentration (solid curves starting from surfaces) obtained from SRIM simulations [15] of Cu/V 50 nm and Cu/V 5 nm nanolaminates by using experimental radiation parameters. The simulated maximum He concentration is ~5 at.% at a depth of around 200 nm underneath film surfaces where the peak displacement per atom (dpa) is approximately 6. XTEM images show that the layer interfaces remain distinct after radiation. Scanning transmission electron microscopy (STEM) studies (not shown here) indicate the retention of chemically abrupt layer interface in the peak damage region in all irradiated specimens. Inserted SAD patterns indicate irradiated films have similar texture as before. Peak damage regions outlined by a box in Fig. 1(c) and (d), are compared in Fig. 1(e) and (f). Careful examination of these figures shows that white dots, typical signatures of He bubbles, appear in both Cu and V. Distributions of He bubble density along the implantation path, obtained from systematic microscopy studies, in Cu/V 50 nm and Cu/V 2.5 nm nanolaminates are shown in Fig. 2.

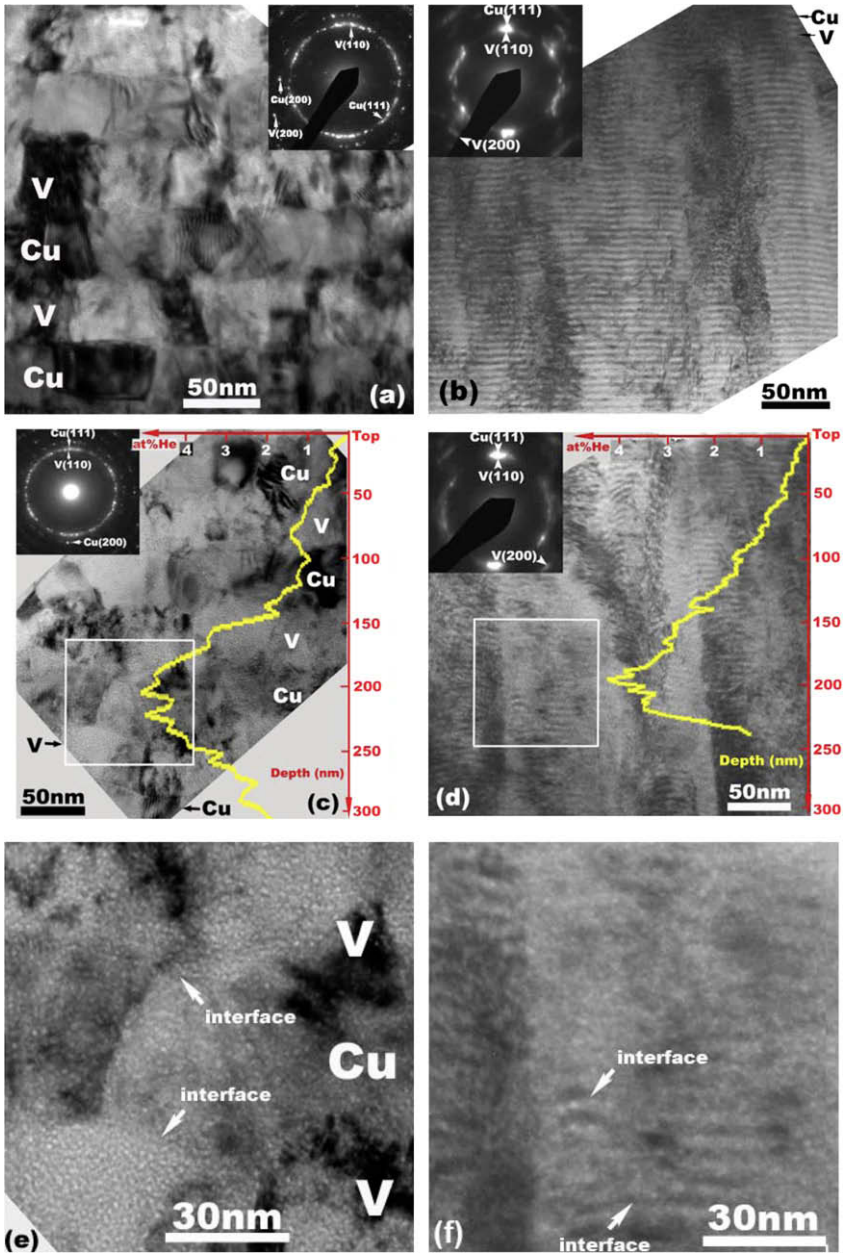

Fig. 1. Cross-sectional bright field TEM images of as-deposited (a) Cu/V 50 nm and (b) Cu/V 2.5 nm, ion irradiated (c) Cu/V 50 nm and (d) Cu/V 2.5 nm nanolaminates. In (c) and (d), peak damage regions as indicated by two square boxes are magnified in (e) and (f), respectively. Interfaces retain in peak damage region with a peak dpa of 6.

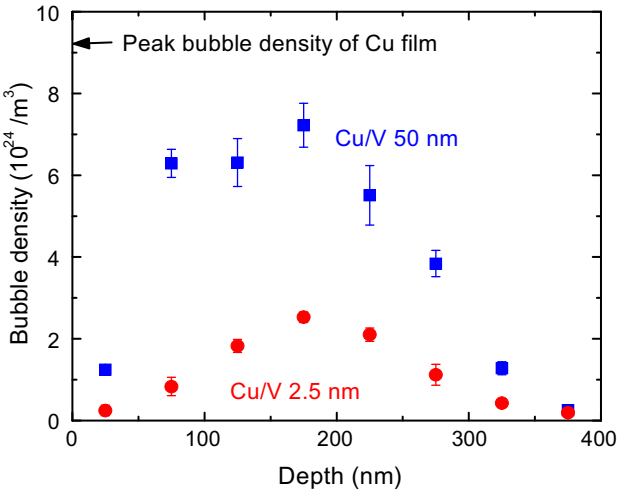

Fig. 2. Helium bubble density as a function of depth from the surface in ion irradiated Cu/V 50 nm and Cu/V 2.5 nm nanolaminates. The maximum bubble density appears approximately 200 nm underneath surfaces in both cases. Both the peak and average He bubble density are higher in Cu/V 50 nm sample.

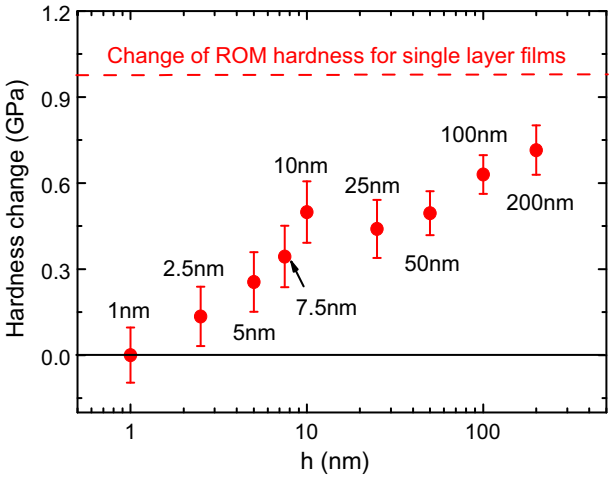

Fig. 3. Hardness change of Cu/V nanolaminates after ion irradiation vs. h, where h is the individual layer thickness. Radiation hardening decreases with decreasing h. Change of rule-of-mixture (ROM) hardness of Cu and V single layer films before and after ion irradiation is also shown by the horizontal dash line.

The maximum bubble density appears approximately 200 nm underneath surfaces in Cu/V 50 nm and Cu/V 2.5 nm, respectively. In Cu/V 50 nm nanolaminate, the peak and average He bubble density are ~3–4 times higher than those in Cu/V 2.5 nm sample. The peak He bubble density in irradiated (under the same He ion energy and fluence) single layer Cu films is also shown in Fig. 2. In all nanolaminates, the peak and average He bubble density are lower than those in irradiated single layer Cu films. Radiation-induced void swelling is also indicated by a 15 nm increase in step height (corresponding to 3.8% of total thickness of the radiated region) as measured by profilometer in irradiated Cu/V 50 nm nanolaminate, comparing to a step height increase of 7 nm (1.8% of total thickness of the radiated region) in irradiated Cu/V 2.5 nm specimen.

The evolution of hardnesses of nanolaminates after ion radiation is examined by nanoindentation studies, and the change of hardness is plotted as a function of h in Fig. 3, where h is individual layer thickness. Significant radiation hardening is observed at greater h, whereas hardnesses barely change at smaller h. To confirm the dependence of radiation hardening on layer thickness, three sets of experiments (different depositions followed by He ion irradiations) were performed and results (not shown here) are reproducible and show the same trend, i.e., less radiation hardening at smaller thickness. The magnitude of radiation hardening, ~1 GPa, in single layer Cu and V films irradiated under identical conditions is higher than that in all Cu/V nanolaminates.

4. Discussions

In He ion irradiated Cu/V nanolaminates, the distribution of He bubble density underneath film surfaces correlates well with SRIM simulated He concentrations. The observation of a significant reduction in He bubble density, and a smaller step height in irradiated Cu/V 2.5 nm specimens, compared to single layer Cu and Cu/V 50 nm specimens, shows that the overall volume of He bubbles and void swelling have been clearly reduced. The reduced void swelling in sputtered Cu/V nanolaminates indicates that vacancy concentration has been dramatically decreased. A large number of vacancies and interstitials may have migrated to interfacial regions where they recombine. If layer interface act as sinks for these point defects, the recombination probability of vacancy-interstitial pairs could vary as a function of distance to layer interface, i.e. recombination probability is higher for defects generated in close proximity to interfaces. Such a proximity effect will be more pronounced in nanolaminates with smaller h. Hence the overall point defect concentration should be lower in Cu/V 2.5 nm specimens than that in Cu/V 50 nm nanolaminates. When h increases even further, greater than 50 nm, the influence of layer interface on recombination of point defect pairs is diminished dramatically and hence the overall bubble density is comparable to that in single layer Cu films. The retention of layer interfaces after radiation, as shown by XTEM studies, indicates that nearly immiscible Cu/V interfaces (a maximum solid solubility of 2.5 wt% Cu in V matrix at 800 °C [16]) are very resistant to He ion irradiation-induced intermixing. Dislocations are shown to be sinks for radiation-induced point defects, and the sink strength of dislocations is proportional to dislocation density. Hence cold working of structural steels, a process that typically induces a higher dislocation density, has been used to enhance the void swelling resistance of alloys to a moderate level [2,17].

Radiation hardening typically occurs concurrently with embrittlement and is generally considered as a gauge to probe the magnitude of radiation damage. In bulk metals, radiation hardening is contributed by interactions of dislocations with different types of defects: strong obstacles, such as precipitates, voids, dislocation loops, and stacking fault tetrahedra, and relatively weak obstacles, such as He bubbles [9,18,19]. A model was developed by Friedel–Kroup–Hirsch (FKH) to estimate hardening from weak obstacles (He bubbles) [20,21]. In this study, the increase in yield strength induced by He bubbles, estimated from FKH model is ~0.08 GPa and 0.03 GPa in Cu/V 50 nm and Cu/V 2.5 nm specimens, respectively, lower than the measured hardness increases, assuming yield strength is ~1/3 of measured hardness. Thus radiation hardening in Cu/V nanolaminates may also result from other types of defects, such as interstitial loops. The reduction of radiation hardening at smaller h presumably indicates that the density of interstitial loops has been reduced in nanolaminates with smaller individual layer thickness.

5. Conclusions

The current study reveals that layer interfaces in nearly immiscible Cu/V nanolaminates play a crucial role in reducing radiation-induced point defects. The helium bubble density is significantly reduced at layer thickness of 2.5 nm and below, indicating a reduction in radiation-induced vacancy concentration. Furthermore, negligible radiation hardening is observed at individual

layer thickness below 2.5 nm, indicating a reduction in radiation-induced interstitial clusters and loops. The study hints that enhancement of radiation tolerance in metal could be achieved by properly designing interface and controlling length scales in metallic nanocomposites.

Acknowledgements

XZ acknowledges financial support by DOE-NERI, Office of Nuclear Energy, Science and Technology, AFCI program, under Grant No. DE-FC07-05ID14657. L. Shao acknowledges the support from NRC Early Career Development Grant. Discussion with Dr K.T. Hartwig is appreciated. The access to a user facility, the Microscopy and Imaging Center at Texas A&M University, is also acknowledged.

References

[1] H. Trinkaus, B.N. Singh, J. Nucl. Mater. 323 (2003) 229.
[2] G.S. Was, Fundamentals of Radiation Materials Science, Springer, Berlin, 2007.
[3] S.J. Zinkle, Phys. Plasmas 12 (2005) 058101.
[4] F.A. Garner, M.B. Toloczko, B.H. Sencer, J. Nucl. Mater. 276 (2000) 123.
[5] S.I. Golubova, B.N. Singh, H. Trinkaus, J. Nucl. Mater. 276 (2000) 78.
[6] D.L. Porter, F.A. Garner, J. Nucl. Mater. 159 (1988) 114.
[7] N. Hashimoto, T.S. Byun, K. Farrell, J. Nucl. Mater. 351 (2006) 295.
[8] K. Shiraishi, K. Fukaya, Y. Katano, J. Nucl. Mater. 54 (1974) 275.
[9] G.E. Lucas, J. Nucl. Mater. 206 (1993) 287.
[10] T. Hochbauer, A. Misra, K. Hattar, R.G. Hoagland, J. Appl. Phys. 98 (2005) 123516.
[11] X. Zhang, Nan Li, O. Anderoglu, H. Wang, J.G. Swadener, T. Hochbauer, A. Misra, R.G. Hoagland, Nucl. Instrum. and Meth. B 261 (2007) 129.
[12] N. Nita, R. Schaeublin, M. Victoria, R.Z. Valiev, Philos. Mag. 85 (2005) 723.
[13] M.J. Demkowicz, R.G. Hoagland, J.P. Hirth, Phys. Rev. Lett. 100 (2008) 136102.
[14] E.G. Fu, Nan Li, A. Misra, R.G. Hoagland, H. Wang, X. Zhang, Mater. Sci Eng. A 493 (2008) 283.
[15] J.F. Ziegler, J.P. Biersack, U. Littmark, The Stopping and Range of Ions in Solids, Pergamon, New York, 1985.
[16] T.B. Massalski, J.L. Murray, L.H. Bennett, H. Baker, Binary Alloy Phase Diagrams, American Society for Metals, Metals Park, Ohio, 1986.
[17] L.K. Mansur, J. Nucl. Mater. 216 (1994) 97.
[18] G.R. Odette, D. Frey, J. Nucl. Mater. 85&86 (1979) 817.
[19] H. Trinkaus, J. Nucl. Mater. 318 (2003) 234.
[20] J. Friedel, Dislocations, Pergamon, New York, 1964.
[21] F. Kroupa, P.B. Hirsch, Disc. Faraday Soc. 38 (1964) 49.